Covalent Metal−Organic Networks: Pyridines Induce 2-Dimensional Oligomerization of (μ-$OC_6H_4O)_2Mpy_2$ (M = Ti, V, Zr)

Joseph M. Tanski, Thomas P. Vaid, Emil B. Lobkovsky, and Peter T. Wolczanski*

Baker Laboratory, Department of Chemistry & Chemical Biology, Cornell University, Ithaca, New York 14853

Received March 30, 2000

Treatment of $M(O^iPr)_4$ (M = Ti, V) and $[Zr(OEt)_4]_4$ with excess 1,4-HOC_6H_4OH in THF afforded $[M(OC_6H_4O)_a(OC_6H_4OH)_{3.34-1.83a}(O^iPr)_{0.66-0.17a}(THF)_{0.2}]_n$ (M = Ti, **1**-Ti; V, **1**-V, $0.91 \le a \le 1.82$) and [Zr-(1,4-$OC_6H_4O)_{2-x}(OEt)_{2x}]_n$ (**1**-Zr, $x = 0.9$). The combination of of **1**-M (M = Ti, V, Zr) or $M(O^iPr)_4$ (M = Ti, V), excess 1,4- or 1,3-HOC_6H_4OH, and pyridine or 4-phenylpyridine at 100 °C for 1 d to 2 weeks afforded various 2-dimensional covalent metal−organic networks: [*cis*-$M(\mu_{1,4}$-$OC_6H_4O)_2py_2]_\infty$ (**2**-M, M = Ti, Zr), [*trans*-$M(\mu_{1,4}$-$OC_6H_4O)_2py_2$·$py]_\infty$ (**3**-M, M = Ti, V), solid solutions [*trans*-$Ti_xV_{1-x}(\mu_{1,4}$-$OC_6H_4O)_2py_2$·$py]_\infty$ (**3**-Ti_xV_{1-x}, $x \approx 0.4$, 0.6, 0.9), [*trans*-$M(\mu_{1,4}$-$OC_6H_4O)_2$(4-Ph-py)$_2]_\infty$ (**4**-M, M = Ti, V), [*trans*-$Ti(\mu_{1,3}$-$OC_6H_4O)_2py_2]_\infty$ (**5**-Ti), and [*trans*-$Ti(\mu_{1,3}$-$OC_6H_4O)_2$(4-Ph-py$)_2]_\infty$ (**6**-Ti). Single-crystal X-ray diffraction experiments confirmed the pleated sheet structure of **2**-Ti, the flat sheet structure of **3**-Ti, and the rippled sheet structures of **4**-Ti, **5**-Ti, and **6**-Ti. Through protolytic quenching studies and by correspondence of powder XRD patterns with known titanium species, the remaining complexes were structurally assigned. With py or 4-Ph-py present, aggregation of titanium centers is disrupted, relegating the building block to the *cis*- or *trans*-$(ArO)_4Tipy_2$ core. The sheet structure types are determined by the size of the metal and the interpenetration of the layers, which occurs primarily through the pyridine residues and inhibits intercalation chemistry.

Introduction

The construction of transition-metal coordination polymers that utilize multifunctional organic ligands is predicated on the plausibility of structural control,[1,2] typically based on stoichiometry.[3] The directionality available in the myriad rigid organic spacers available contrasts dramatically with the elemental components of inorganic solid-state compounds and, in theory, permits common structural types to be engineered.[4]

Covalent, metal−organic networks (CMONs) derived from early transition metals and dialkoxyaromatic spacers constitute an unusual subclass of coordination polymers, because their connectivity is not based on dative[1−4] or hydrogen bonding.[5,6] Covalent linkages[7] are generated via alcoholyis reactions, and once coordination geometries of the metals have been established, common structural motifs ensue. For example, edge-shared, bioctahedral dititanium building blocks (e.g., [(−$OC_6H_4O)_2$(HOC_6H_4O)(−OC_6H_4OH)Ti]$_2$(μ-$OC_6H_4OH)_2$)[8,9] prevail in solvents of low donor capacity. A bioctahedron has 10 potential connecting sites: four axial, four equatorial, and two bridging. Networks that possess body-centered and hexagonal motifs require eight covalent linkages emanating from the bioctahedron,[8,9] and primitive frameworks need six connections between adjacent dititanium centers.[10] In some instances, a restricted linking ability of the spacer has led to a reduction from 3- to 2-dimensionality (e.g., {[Ti($\mu_{1,3}$-1,3-OC_6H_4O)(μ-1,3-OC_6H_4-OH)(1,3-OC_6H_4OH)(HO^iPr)]$_2$}$_n$),[10] even in nondonor solvents.[10]

Donor solvents and added ligands may be used to lower the dimensionality of CMON materials that are based on early transition metals and dialkoxyaromatic components. For example, the use of pyridines obviates aggregation via μ-aryloxide (μ-OAr) bridges, and restricts polymerization to two dimensions, where *cis*- and *trans*-$(ArO)_4Mpy_2$ geometries and specific constraints of the ligands lead to flat, rippled, or pleated sheet[9] structures. Herein are described the syntheses of various 2-dimensional titanium, vanadium, and zirconium compounds based on 1,3- and 1,4-dialkoxybenzene in combination with pyridine and 4-phenylpyridine, and several structures where M = Ti.

Results

Syntheses. CMON derivatives are typically prepared by two routes: (1) the dihydroxyaromatic (DHA) and an amorphous oligomeric material generated from a molecular precursor and

(1) Janiak, C. *Angew. Chem., Int. Ed. Engl.* **1997**, *36*, 1431−1434.
(2) For pertinent recent examples, see: (a) Gardner, G. B.; Venkataraman, D.; Moore, J. S.; Lee, S. *Nature* **1995**, *374*, 792−795. (b) Yaghi, O. M.; Li, G. *Angew. Chem., Int. Ed. Engl.* **1995**, *34*, 207−209. (c) Abrahams, B. F.; Batten, S. R.; Hamit, H.; Hoskins, B. F.; Robson, R. *J. Chem. Soc., Chem. Commun.* **1996**, 1313−1314. (d) Hennigar, T. L.; MacQuarrie, D. C.; Losier, P.; Rogers, R. D.; Zaworotko, M. J. *Angew. Chem., Int. Ed. Engl.* **1997**, *36*, 972−973. (e) Noro, S.; Kondo, M.; Ishii, T.; Kitagawa, S.; Matsuzaka, H. *J. Chem. Soc., Dalton Trans.* **1999**, 1569−1574. (f) Carlucci, L.; Ciani, G.; Proserpio, D. M. *J. Chem. Soc., Dalton Trans.* **1999**, 1799−1804.
(3) Zaworotko, M. J. *Angew. Chem., Int. Ed. Engl.* **1998**, *37*, 1211−1213.
(4) (a) Hoskins, B. F.; Robson, R. *J. Am. Chem. Soc.* **1990**, *112*, 1546−1554. (b) Power, K. N.; Hennigar, T. L.; Zaworotko, M. J. *J. Chem. Soc., Chem. Commun.* **1998**, 595−596. (c) Niu, T.; Wang, X.; Jacobson, A. J. *Angew. Chem., Int. Ed. Engl.* **1999**, *38*, 1934−1936.
(5) Desiraju, G. R. *Angew. Chem., Int. Ed. Engl.* **1995**, *34*, 2311−2327.
(6) Evans, C. C.; Sukarto, L.; Ward, M. C. *J. Am. Chem. Soc.* **1999**, *121*, 320−325 and references therein.
(7) Haaland, A. *Angew. Chem., Int. Ed. Engl.* **1989**, *28*, 992−1007.
(8) Vaid, T. P.; Tanski, J. M.; Pette, J. M.; Lobkovsky, E. B.; Wolczanski, P. T. *Inorg. Chem.* **1999**, *38*, 3394−3405.
(9) Vaid, T. P.; Lobkovsky, E. B.; Wolczanski, P. T. *J. Am. Chem. Soc.* **1997**, *119*, 874−875.
(10) Tanski, J. M.; Lobkovsky, E. B.; Wolczanski, P. T. *J. Solid State Chem.* **2000**, *152*, 130−140.

10.1021/ic0003473 CCC: $19.00
Published on Web 09/19/2000

the DHA are heated in a sealed tube with an appropriate donor, and (2) a molecular precursor and the DHA are directly heated in a sealed tube with a potential donor ligand.[8] The use of the amorphous oligomeric material aids in lowering the probability that ligands of the molecular precursor become incorporated in the CMON. With the pyridine derivatives described below, the likelihood of this occurrence was deemed to be small, and while both methods were used, the easier direct preparation of CMONs often proved suitable.

Treatment of $M(O^iPr)_4$ (M = Ti, V) with 2.58 equiv of 1,4-HOC_6H_4OH in THF afforded red-orange and black powders, respectively, after trituration with hexanes and drying. A rough

$$M(^iOPr)_4 + 2.58HOC_6H_4OH \xrightarrow{\text{THF, 25 °C}} (1/n)[Ti(OC_6H_4O)_a(OC_6H_4OH)_{3.34-1.83a}(O^iPr)_{0.66-0.17a}(THF)_{0.2}]_n + (3.34 + 0.17a)HO^iPr \quad (1)$$

M = Ti, **1**-Ti; V, **1**-V ($0.91 \le a \le 1.82$)

composition of the Ti derivative was determined from elemental analyses and ^{1}H NMR spectral assays of its acid hydrolysis degradation products as previously described.[8] Although repetitive elemental analyses were not conducted on **1**-V, decomposition from addition of DCl/D_2O produced DOC_6H_4OD:DO^iPr:THF ratios consistent with a formulation similar to **1**-Ti, according to ^{1}H NMR spectral analyses. The modified sol−gel preparations of these amorphous (powder XRD), oligomeric precursors were based on related materials synthesized by Burch.[11]

A related colorless precursor precipitated when $[Zr(OEt)_4]_4$ and 1,4-HOC_6H_4OH were allowed to mix in THF. In contrast

$$[Zr(OEt)_4]_4 + \underset{\text{(excess)}}{1,4\text{-}HOC_6H_4OH} \xrightarrow[\text{THF}]{\text{22 °C}} [Zr(1,4\text{-}OC_6H_4O)_{2-x}(OEt)_{2x}]_n \quad (2)$$

1-Zr, $x = 0.9$

to **1**-M (M = Ti, V), DCl/D_2O quenching studies indicated that $[Zr(1,4\text{-}OC_6H_4O)_{2-x}(OEt)_{2x}]_n$ (**1**-Zr, $x = 0.9$) contained substantial quantities of ethoxide, and its stoichiometry revealed little or no semiquinone. Although the composition of **1**-Zr is very close to $[Zr(1,4\text{-}OC_6H_4O)(OEt)_2]_n$, crystallization of this material could not be effected despite numerous attempts.

A combination of excess hydroquinone and **1**-Ti in py at 100 °C for 1−4 d produced either red-orange [*cis*-Ti($\mu_{1,4}$-$OC_6H_4O)_2py_2]_\infty$ (**2**-Ti, eq 3) or dark green [*trans*-Ti($\mu_{1,4}$-$OC_6H_4O)_2py_2$·$py]_\infty$ (**3**-Ti, eq 4) depending on the concentration of 1,4-HOC_6H_4OH. At ~1.82 M, the *cis* derivative was produced exclusively, while the *trans* compound was generated at ~0.55 M. The ligand stoichiometries were determined via ^{1}H NMR analyses of DCl/D_2O quenches, and the powder XRD of each bulk material proved to be consistent with the theoretical pattern generated from single-crystal X-ray diffraction data. When a sample of **3**-Ti was subjected to the conditions (100 °C, 2 d) used to prepare **2**-Ti, it was converted to the *cis* material,

$$\underset{\textbf{3}\text{-Ti}}{[\textit{trans}\text{-}Ti(\mu_{1,4}\text{-}OC_6H_4O)_2py_2\cdot py]_\infty} \underset{}{\overset{py}{\rightleftharpoons}} \underset{\textbf{2}\text{-Ti}}{[\textit{cis}\text{-}Ti(\mu_{1,4}\text{-}OC_6H_4O)_2py_2]_\infty} \quad (5)$$

whereas **2**-Ti could not be converted to the *trans* compound when placed in a ~0.55 M pyridine solution of hydroquinone under similar conditions. The crystallization (100 °C) of **3**-Ti at an intermediate concentration of hydroquinone (1.36 M) was monitored by powder XRD over the course of several days. After 22 h, only **3**-Ti was present, and over the next 13 d it remained the predominant phase, with only a trace of **2**-Ti appearing during the latter stages. The reaction mixture was then heated to 150 °C for 44 h, and powder XRD revealed a **2**-Ti:**3**-Ti ratio of ~19:1. These experiments suggest that the thermodynamically more stable solid is the *cis* material, but that the *trans* compound is more readily formed (i.e., the kinetic product), and the amount of 1,4-HOC_6H_4OH in solution plays a key role in determining their formation and interconversion.

Only very small crystals (<5 μm per side) of **3**-Ti were obtained through eq 4, but an attempt to prepare Ti(III) derivatives serendipitously led to slightly larger crystals that proved amenable to single-crystal X-ray diffraction analysis. First, an orange-brown precursor, $Ti(OC_6H_4O)_{1.5-x}(N(SiMe_3)_2)_{2x}(THF)_{\sim 0.6}$ (pre-**3**-Ti, $2x \approx 0.03$) derived from Ti-$[N(SiMe_3)_2]_3$ and 1,4-HOC_6H_4OH was prepared (eq 6). A rough hydroquinone-to-amine ratio was determined by degradation in DCl/D_2O and analysis by ^{1}H NMR spectroscopy, but the actual oxidation state(s) of the titanium was not determined. Excess hydroquinone, pre-**3**-Ti, and pyridine were then heated in a glass tube for 3 d at 85 °C to afford **3**-Ti (eq 7), whose larger crystals

$$Ti[N(SiMe_3)_2]_3 + 1,4\text{-}HOC_6H_4OH \xrightarrow[\text{THF}]{\text{22 °C, 7 h}} \sim 3HN(SiMe_3)_2 + \underset{\text{pre-}\textbf{3}\text{-Ti, } 2x \approx 0.03}{Ti(OC_6H_4O)_{1.5-x}(N(SiMe_3)_2)_{2x}(THF)_{\sim 0.6}} \quad (6)$$

$$\underset{\text{(excess)}}{\text{pre-}\textbf{3}\text{-Ti} + 1,4\text{-}HOC_6H_4OH} \xrightarrow[\text{py}]{\text{85 °C, 3 d}} \underset{\textbf{3}\text{-Ti}}{[\textit{trans}\text{-}Ti(\mu_{1,4}\text{-}OC_6H_4O)_2py_2\cdot py]_\infty} \quad (7)$$

possessed a lustrous gold appearance amid the forest green of the remaining material. A powder XRD analysis of the bulk revealed it to be **3**-Ti, and a ^{1}H NMR spectrum of the material degraded by DCl/D_2O confirmed the 2:3 ratio of hydroquinone to pyridine. The actual composition of pre-**3**-Ti, and the redox chemistry involved in the overall conversion of $Ti^{III}[N(SiMe_3)_2]_3$ to **3**-Ti^{IV} render it difficult to envision a discrete mechanism for the transformation, but stoichiometry is likely to be that described by eq 8.

$$2Ti[N(SiMe_3)_2]_3 + 4HOC_6H_4OH + 6py \rightarrow \underset{\textbf{3}\text{-Ti}}{2[\textit{trans}\text{-}Ti(\mu_{1,4}\text{-}OC_6H_4O)_2py_2\cdot py]_\infty} + H_2 + 6HN(SiMe_3)_2 \quad (8)$$

(11) Burch, R. R. *Chem. Mater.* **1990**, *2*, 633−634.

Upon thermolysis (100 °C, 13 d) of **1**-V and hydroquinone (3.4 M) in pyridine, dark green-black [*trans*-V($\mu_{1,4}$-$OC_6H_4O)_2$-py_2·py]$_\infty$ (**3**-V) was obtained (eq 9). Again, DCl/D_2O quenching

$$\underset{(3.4\ \mathrm{M})}{\textbf{1}\text{-M} + 1,4\text{-HOC}_6\text{H}_4\text{OH}} \xrightarrow[\text{py}]{100\ ^\circ\text{C, 13 d}} \underset{\textbf{3}\text{-V}}{[\textit{trans}\text{-V}(1,4\text{-OC}_6\text{H}_4\text{O})_2\text{py}_2\cdot\text{py}]_\infty} \quad (9)$$

studies were used to augment powder XRD data that suggested a composition and structure analagous to **3**-Ti. The size of the crystals of **3**-V was <5 μm, and various attempts failed to yield larger material. Magnetic susceptibility measurements showed the d^1-based compound to behave as a simple paramagnet from 2 to 298 K ($\mu = 2.05\ \mu_B$).

Since the powder XRD pattern of [*trans*-V($\mu_{1,4}$-$OC_6H_4O)_2$-py_2·py]$_\infty$ (**3**-V) was indexed to a cell quite similar to that of [*trans*-Ti($\mu_{1,4}$-$OC_6H_4O)_2py_2$·py]$_\infty$ (**3**-Ti), and the metal radii (r_{cov}(Ti) = 1.32 Å, r_{cov}(V) = 1.22 Å)[12] are the only tangible structural parameters that are different, the preparation of solid solutions seemed logical. Treatment of 1:3, 1:1, and 3:1 mixtures of **3**-Ti and **3**-V with hydroquinone in pyridine resulted in the synthesis of [*trans*-Ti_xV_{1-x}($\mu_{1,4}$-$OC_6H_4O)_2py_2$·py]$_\infty$ (**3**-Ti_xV_{1-x}, $x \approx 0.4, 0.6, 0.9$). Analysis of a D_2O/DCl quench of each solid

$$\underset{y = 0.25, 0.50, 0.75}{y\textbf{3}\text{-Ti} + (1-y)\textbf{3}\text{-V}} + \underset{(\text{excess})}{1,4\text{-HOC}_6\text{H}_4\text{OH}} \xrightarrow[2\text{ d, py}]{100\ ^\circ\text{C}} \underset{\textbf{3}\text{-Ti}_x\text{V}_{1-x},\ x \approx 0.4, 0.6, 0.9}{[\textit{trans}\text{-Ti}_x\text{V}_{1-x}(\mu_{1,4}\text{-OC}_6\text{H}_4\text{O})_2\text{py}_2\cdot\text{py}]_\infty} \quad (10)$$

solution afforded the expected 2:3 ratio of DOC_6H_4OD to py, and powder XRD patterns revealed deviations from the pure materials. Figure 1 illustrates the 6−26° region in 2θ, and manifests subtle changes in the low-angle region, while distinct lines emerge around 20−22° in 2θ as the percentage of Ti is increased. An overnight powder XRD pattern of **3**-$Ti_{0.6}V_{0.4}$ provided data of quality sufficient for indexing, and the unit cell volume was consistent with the solid solution formulation. The value of 626.8 $Å^3$ was between the volumes obtained for **3**-Ti (632.6 $Å^3$) and **3**-V (622.5 $Å^3$) that were also obtained from room-temperature powder XRD data. Electron microprobe analysis of single crystals of **3**-$Ti_{0.6}V_{0.4}$ as well as a bulk analysis showed consistent Ti:V ratios; the remaining pair of solid solutions were only analyzed in the bulk.

The combination of **1**-Zr, hydroquinone (1.1 M), and pyridine provided colorless [*cis*-Zr($\mu_{1,4}$-$OC_6H_4O)_2py_2]_\infty$ (**2**-Zr) after 7 d at 100 °C (eq 11). Powder XRD afforded a clean pattern which

$$\underset{(1.82\ \mathrm{M})}{\textbf{1}\text{-Zr} + 1,4\text{-HOC}_6\text{H}_4\text{OH}} \xrightarrow[\text{py}]{100\ ^\circ\text{C, 7 d}} \underset{\textbf{2}\text{-Zr}}{[\textit{cis}\text{-Zr}(\mu_{1,4}\text{-OC}_6\text{H}_4\text{O})_2\text{py}_2]_\infty} \quad (11)$$

corresponded to that obtained for **2**-Ti, and DCl/D_2O quenching studies revealed a 1:1 ratio of hydroquinone to pyridine.

Prolonged heating (100 °C) of [*trans*-Ti($\mu_{1,4}$-$OC_6H_4O)_2py_2$·py]$_\infty$ (**3**-Ti) in benzene or THF solution permitted ~80% and 100% exchange of the lattice-bound pyridine for the solvent, respectively, according to the DCl/D_2O quenching studies. The failure to intercalate various aromatic organics and common organometallics (e.g., Cp_2Co) into either **3**-Ti or **2**-Ti prompted

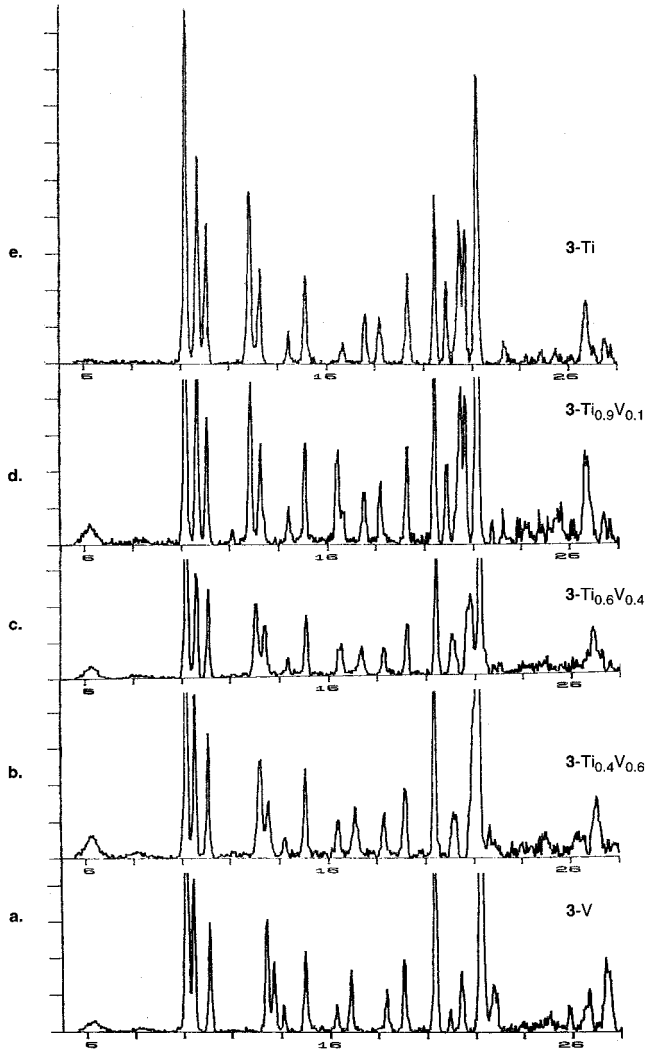

Figure 1. Powder XRD patterns for [*trans*-V($\mu_{1,4}$-$OC_6H_4O)_2py_2$·py]$_\infty$ (**3**-V (a)), the solid solutions Ti_xV_{1-x}($\mu_{1,4}$-$OC_6H_4O)_2py_2$·py]$_\infty$ (**3**-Ti_xV_{1-x}, $x \approx 0.4$ (b), 0.6 (c), 0.9 (d)), and [*trans*-Ti($\mu_{1,4}$-$OC_6H_4O)_2py_2$·py]$_\infty$ (**3**-Ti, (e)).

investigations into other means to separate the layers of the material.[13] As a consequence, 4-phenylpyridine, hydroquinone, and M(O^iPr)$_4$ (M = Ti, V) were heated to 100 °C in a sealed tube for several days, and microcrystalline material appeared (eq 12). After 2 months, red-orange crystals (~20%) of [*trans*-

$$\underset{(\text{excess})}{\mathrm{M(O^iPr)_4} + 1,4\text{-HOC}_6\text{H}_4\text{OH}} + \underset{(\text{excess})}{4\text{-Ph-py}} \xrightarrow{100\ ^\circ\text{C}} \underset{\textbf{4}\text{-Ti; V, }\textbf{4}\text{-V}}{[\textit{trans}\text{-M}(\mu_{1,4}\text{-OC}_6\text{H}_4\text{O})_2(4\text{-Ph-py})_2]_\infty} \quad (12)$$

Ti($\mu_{1,4}$-$OC_6H_4O)_2$(4-Ph-py)$_2]_\infty$ (**4**-Ti) suitable for X-ray diffraction analysis were harvested amidst a dark powder. The dark powder was considered amorphous because DCl/D_2O quenching studies indicated a 2:3 ratio of hydroquinone to 4-Ph-py. The ratio was incommensurate with the 2-dimensional layered structure obtained for **4**-Ti, despite a powder XRD of the bulk material that corresponded to the theoretical pattern calculated from the single-crystal data. Likewise, yellow crystals (~50%) of [*trans*-V($\mu_{1,4}$-$OC_6H_4O)_2$(4-Ph-py)$_2]_\infty$ (**4**-V) were also separated from a dark opaque powder. A DCl/D_2O quench of the

(12) Pauling, L. *The Nature of the Chemical Bond*, 3rd ed.; Cornell University Press: Ithaca, New York, 1960.

(13) O'Hare, D. In *Inorganic Materials*; Bruce, D. W., O'Hare, D., Eds.; John Wiley & Sons: New York, 1992; pp 165−235.

mixture revealed a 2:2.25 ratio of DOC_6H_4OD to 4-Ph-py, while the powder XRD showed a one-to-one correspondence with the theoretical powder pattern generated from the single-crystal study of **4**-Ti. The inequities in ligand ratios from the quench, when combined with the powder XRD analysis in conjunction with the single-crystal X-ray study of **4**-Ti, suggest that the dark powders are amorphous and possess hydroquinone to 4-Ph-py ratios $\geq$2:3.

Despite the extension of the aromatic residues via the use of the 4-phenyl-substituted pyridine, features of the layered structures of **4**-Ti and **4**-V apparently hamper intercalation; attempts to swell the materials with aromatic hydrocarbons failed. Reasoning that irregularities in the 2-dimensional sheets of these materials, i.e., rippling, might disturb the lamellar energetics, a switch from hydroquinone to resorcinol, 1,3-HOC_6H_4OH, was made. Treatment of $Ti(O^iPr)_4$ with a >10-fold excess of resorcinol in pyridine afforded red crystals of [*trans*-$Ti(\mu_{1,3}\text{-}OC_6H_4O)_2py_2]_\infty$ (**5**-Ti) after only 2 d at 100 °C (eq 13). A ^1H NMR spectrum of a DCl/D_2O quench revealed a

$$\underset{\text{(excess)}}{Ti(O^iPr)_4 + 1,3\text{-}HOC_6H_4OH} \xrightarrow[\text{py}]{100\ ^\circ C,\ 2\ d} \underset{\textbf{5}\text{-Ti}}{[\textit{trans}\text{-}Ti(\mu_{1,3}\text{-}OC_6H_4O)_2py_2]_\infty} \quad (13)$$

1:1 ratio of 1,3-DOC_6H_4OD to py, and the powder XRD of the bulk material matched the theoretical pattern obtained from the single-crystal X-ray diffraction data.

When intercalation efforts with **5**-Ti were also unsuccessful, a combination of resorcinol and the larger pyridine spacer was used. When $Ti(O^iPr)_4$, 4-phenylpyridine, and resorcinol were heated for 4 weeks at 100 °C, deep red crystals of [*trans*-$Ti(\mu_{1,3}\text{-}OC_6H_4O)_2(4\text{-Ph-py})_2]_\infty$ (**6**-Ti) were generated (eq 14).

$$\underset{\text{(excess)}}{Ti(O^iPr)_4 + 1,3\text{-}HOC_6H_4OH} \xrightarrow[\text{py}]{100\ ^\circ C,\ 4\ wk} \underset{\textbf{6}\text{-Ti}}{[\textit{trans}\text{-}Ti(\mu_{1,3}\text{-}OC_6H_4O)_2(4\text{-Ph-py})_2]_\infty} \quad (14)$$

Again, the 1:1 ratio of spacer (resorcinol) to donor (4-Ph-py) was established by quenching studies, and the powder XRD of the bulk material matched that calculated from the single-crystal X-ray diffraction data of **6**-Ti. No intercalation chemistry was noted for **6**-Ti either.

X-ray Structural Studies. 1. Generalities. Primarily due to crystalline size, only the following Ti derivatives were analyzed by single-crystal X-ray diffraction: [*cis*-$Ti(\mu_{1,4}\text{-}OC_6H_4O)_2py_2]_\infty$ (**2**-Ti), [*trans*-$Ti(\mu_{1,4}\text{-}OC_6H_4O)_2py_2\cdot py]_\infty$ (**3**-Ti), [*trans*-$Ti(\mu_{1,4}\text{-}OC_6H_4O)_2(4\text{-Ph-py})_2]_\infty$ (**4**-Ti), [*trans*-$Ti(\mu_{1,3}\text{-}OC_6H_4O)_2py_2]_\infty$ (**5**-Ti), and [*trans*-$Ti(\mu_{1,3}\text{-}OC_6H_4O)_2(4\text{-Ph-py})_2]_\infty$ (**6**-Ti). Table 1. provides pertinent crystallographic data on the 2-dimensional materials. While powder XRD data often showed that compounds based on V or Zr were highly crystalline (typically <5 μm per side) and pure—at least by the criteria of powder pattern comparison with structurally characterized, homologous Ti species—none of these materials produced crystals of the quality and size necessary for single-crystal analysis, even considering the availability of synchrotron radiation.[8,9]

An inverse correlation of density to the C/N:Ti ratio is not apparent, indicating that the nuances of primary and secondary structure in the five compounds sometimes result in significant void space. The compounds predicted to be the most dense according to their relatively low C/N:Ti ratios of 24, **2**-Ti and **5**-Ti, have densities of 1.406 and 1.480 g/cm^3, respectively,

Table 1. X-ray Crystallographic Data for 2-D CMON Derivatives (Crystal Data, Data Collection, and Refinement)

	[$Ti_2(\mu_{1,4}$-$OC_6H_4O)_2py_2]_\infty$ (**2**-*cis*-Ti)	[$Ti_2(\mu_{1,4}$-$OC_6H_4O)_2py_2\cdot py]_\infty$ (**2**-*trans*-Ti)	[$Ti_2(\mu_{1,4}$-$OC_6H_4O)_2(4\text{-Ph-py})_2]_\infty$ (**4**-Ti)	[$Ti_2(\mu_{1,3}$-$OC_6H_4O)_2py_2]_\infty$ (**5**-Ti)	[$Ti_2(\mu_{1,3}$-$OC_6H_4O)_2(4\text{-Ph-py})_2]_\infty$ (**6**-Ti)
empirical formula	$C_{22}H_{18}N_2O_4Ti$	$C_{13.5}H_{11.5}N_{1.5}O_2Ti_{0.5}$	$C_{34}H_{26}N_2O_4Ti$	$C_{22}H_{18}N_2O_4Ti$	$C_{51}H_{39}N_3O_6Ti_{1.5}$
fw	422.30	250.70	574.50	422.30	861.75
cryst syst	orthorhombic	triclinic	monoclinic	triclinic	monoclinic
space group	*Pmma*	$P\bar{1}$	$P2_1/c$	$P\bar{1}$	$P2_1/c$
Z	4	2	2	2	4
a, Å	15.631(3)	8.679(2)	11.589(2)	8.422(2)	12.843(3)
b, Å	14.017(3)	8.721(2)	8.1029(10)	10.258(2)	29.449(6)
c, Å	9.063(2)	8.978(2)	15.384(2)	10.980(2)	10.963(2)
α, deg	90	82.50(3)	90	91.06(3)	90
β, deg	90	73.78(3)	110.595(3)	91.28(3)	96.91(3)
γ, deg	90	70.24(3)	90	91.65(3)	90
V, Å^3	1985.7(7)	613.6(2)	1352.3(3)	947.8(3)	4116.3(14)
D(calcd), g·cm^{-3}	1.406	1.357	1.411	1.480	1.390
abs coeff, mm^{-1}	0.462	0.387	0.360	0.484	0.355
cryst size, μm	35 × 30 × 25	130 × 95 × 40	90 × 50 × 50	160 × 140 × 50	250 × 200 × 200
temp, K	110(2)	146(2)	293(2)	293(2)	173(2)
radiation, λ, Å	0.9140 (synchrotron)	0.710 73	0.710 73	0.710 73	0.710 73
GOF[a] on F^2	1.224	1.255	0.989	0.994	1.139
R indices[b] [$I > 2\sigma(I)$]	R1 = 0.0846, wR2 = 0.2329	R1 = 0.1425, wR2 = 0.2834	R1 = 0.0558, wR2 = 0.1195	R1 = 0.1085, wR2 = 0.2813	R1 = 0.0512, wR2 = 0.1113
R indices[b] (all data)	R1 = 0.0858, wR2 = 0.2338	R1 = 0.2110, wR2 = 0.3099	R1 = 0.1308, wR2 = 0.1653	R1 = 0.1469, wR2 = 0.3045	R1 = 0.1105, wR2 = 0.1630

[a] GOF = $[\sum w(|F_o| - |F_c|)^2/(n-p)]^{1/2}$; n = number of independent reflections, p = number of parameters. [b] R1 = $\sum||F_o| - |F_c||/\sum|F_o|$; wR2 = $[\sum w(|F_o| - |F_c|)^2/\sum\omega F_o^2]^{1/2}$.

Table 2. Core Bond Distances (Å) and Angles (deg) for [*cis*-Ti($\mu_{1,4}$-$OC_6H_4O)_2py_2]_\infty$ (**2**-Ti), [*trans*-Ti($\mu_{1,4}$-$OC_6H_4O)_2py_2$·py]$_\infty$ (**3**-Ti), [*trans*-Ti($\mu_{1,4}$-$OC_6H_4O)_2$(4-Ph-py)$_2]_\infty$ (**4**-Ti), [*trans*-Ti($\mu_{1,3}$-$OC_6H_4O)_2py_2]_\infty$ (**5**-Ti), and [*trans*-Ti($\mu_{1,3}$-$OC_6H_4O)_2$(4-Ph-py)$_2]_\infty$ (**6**-Ti)

param	**2**-Ti[a]	**3**-Ti	**4**-Ti	**5**-Ti	**6**-Ti
d(TiN)	2.316 (6)	2.183 (9)	2.205 (5)	2.191 $(12)_{av}$	2.199 $(9)_{av}$
d(TiO)	1.895 $(28)_{av}$[t]	1.863 $(26)_{av}$	1.884 $(21)_{av}$	1.874 $(18)_{av}$	1.879 $(8)_{av}$
	1.883 (4)[c]				
d(NC)	1.370 $(9)_{av}$	1.320 $(28)_{av}$	1.326 $(9)_{av}$	1.324 $(24)_{av}$	1.341 $(2)_{av}$
d(OC)	1.365 $(10)_{av}$[t]	1.348 $(2)_{av}$	1.365 $(7)_{av}$	1.344 $(24)_{av}$	1.346 $(5)_{av}$
	1.372 (8)[c]				
∠(NTiO)	84.1 $(16)_{av}$[t]	90.0 $(9)_{av}$	90.0 $(3)_{av}$	89.9 $(6)_{av}$	90.0 $(17)_{av}$
	85.9 (2)[c]				
	170.6 (2)[c]				
∠(NTiN)	84.9 (3)	180.0	180.0	180.0	177.5 (1)
					180.0
∠(OTiO)	95.1 $(11)_{av}$	90.0 $(6)_{av}$	90.0 $(41)_{av}$	90.0 $(10)_{av}$	90.0 $(14)_{av}$
	103.3 (3)[c]	180.0	180.0	180.0	177.5 $(1)_{av}$
	163.7 (3)[t]				180.0
∠(TiNC)	121.9 (34)	122.7 $(28)_{av}$	122.0 $(11)_{av}$	121.1 $(8)_{av}$	121.4 $(13)_{av}$
∠(TiOC)	137.4 (4)[t]	146.6 $(98)_{av}$	145.7 $(38)_{av}$	149.8 $(34)_{av}$	150.1 $(54)_{av}$
	143.3 (6)[c]				
	161.0 (5)[c]				

[a] Superscripts refer to mutually *trans* ([t]) or *cis* ([c]) aryloxide functionalities.

suggesting that the more restricted linkages of the $\mu_{1,3}$-OC_6H_4O spacer help densify the network. Without the pyridine of crystallization, the density of the **3**-Ti network would be only ~1.14 g/cm^3, based on the existing cell. It is plausible that the 1,4-disposition of the aryloxide functionalities on the $\mu_{1,4}$-OC_6H_4O spacer creates too much void space; thus, the network must add an additional pyridine. Inevitably, **3**-Ti loses its intercalated pyridine and collapses to the more dense *cis* structure. If the preponderance of *trans* core geometries is an indication of a subtle enthalpic preference, then entropically favored loss of lattice pyridine from **3**-Ti and the corresponding densification of the network provide the thermodynamic impetus toward **2**-Ti. Despite a C/N:Ti ratio of 30, **3**-Ti is significantly less dense (1.357 g/cm^3) than **4**-Ti (1.411 g/cm^3) and **6**-Ti (1.390 g/cm^3), whose C/N:Ti ratios of 36 are the greatest of the five. Note that the latter two densities contradict the earlier observation that the $\mu_{1,3}$-OC_6H_4O spacer promotes networks that are more dense. It may be that the more dense 2-dimensional sheet disrupts the interpenetration of the 4-Ph-py ligands in this instance.

Of the five structurally characterized compounds, all but **2**-Ti possess a *trans*-$(ArO)_4Tipy_2$ geometry at the core. As a consequence, core structural details of **2**-Ti will be separate from the *trans*-$(ArO)_4Tipy_2$ cases, which can effectively be treated as a group.

2. [*cis*-Ti($\mu_{1,4}$-$OC_6H_4O)_2py_2]_\infty$ (2-Ti). Synchrotron data aquisition and structure solution revealed a 2-dimensional, pleated sheet structure for [*cis*-Ti($\mu_{1,4}$-$OC_6H_4O)_2py_2]_\infty$ (**2**-Ti), which has been briefly described in a previous communication.[9] A strand of *trans*-1,4-diphenoxides (∠(O1−Ti−O2) = 163.7(3)°, ∠(Ti−O1−C6) = 143.3(6)°, ∠(Ti−O2−C9) = 161.0(5)°, *d*(Ti−O1) = 1.915(6) Å, *d*(Ti−O2) = 1.875(6) Å) connect distorted octahedral titanium centers (Table 2, Figure 2a) in one dimension. In another, a zigzag chain of *cis*-1,4-diphenoxides (∠(O3−Ti−O3A) = 103.3(3)°, ∠(Ti−O3−C12) = 137.4(4)°, *d*(Ti−O3) = 1.883(4) Å) establishes a second connectivity (Figure 2b) to complete the 2-dimensional network. *cis*-Pyridines (*d*(Ti−N) = 2.316(6) Å, ∠(N1−Ti−N1A) = 84.9(3)°) alternate with the arenes of the *cis*-1,4-diphenoxide chain to efficiently pack the sheets together, but no evidence for π-stacking is apparent.

3. [*trans*-Ti(μ-$OC_6H_4O)_2L_2]_\infty$ Cores. The four *trans*-Ti(μ-$OC_6H_4O)_2L_2$ compounds exhibit normal octahedral coordination geometries about the titanium (Table 2, Figure 3). The quality

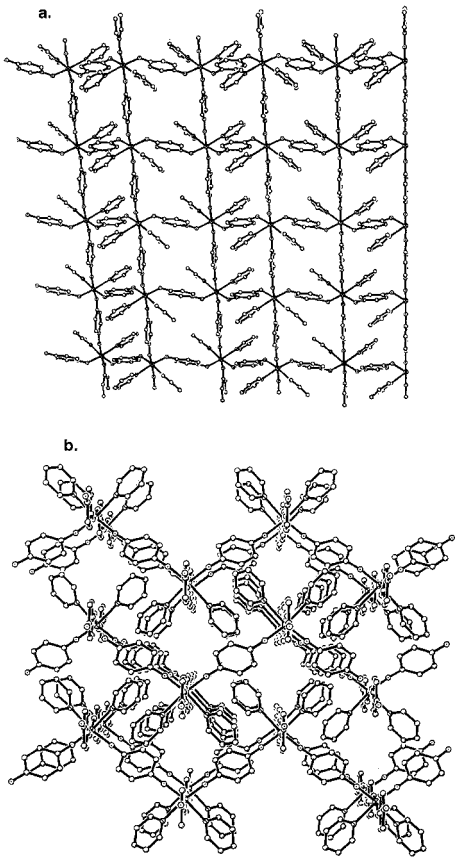

Figure 2. Views of [*cis*-Ti($\mu_{1,4}$-$OC_6H_4O)_2py_2]_\infty$ (**2**-Ti) showing the *trans*-1,4-OC_6H_4O connectivity (a) and the *cis*-1,4-OC_6H_4O linkages and pyridine interpenetration (b).

of the data pertaining to [*trans*-Ti($\mu_{1,4}$-$OC_6H_4O)_2py_2$·py]$_\infty$ (**2**-Ti) was somewhat poorer than that of the related derivatives, but the core bond distances and angles obtained from the model are essentially those of the remaining *trans* complexes; hence, it is included in the general analysis. In terms of the core, the py and 4-Ph-py ligands are not statistically different for the four compounds, nor are the 1,3- and 1,4-OC_6H_4O ligands, as evidenced by *d*(TiN) = 2.195$(10)_{av}$ Å and *d*(TiO) = 1.876-$(15)_{av}$ Å. The bond angles reveal little distortion, with ∠(NTiO) = 89.9$(12)_{av}$°, ∠(OTiO) = 90.0$(15)_{av}$° and 179.4-$(11)_{av}$°, and ∠(NTiN) = 179.6$(10)_{av}$°. While it might be

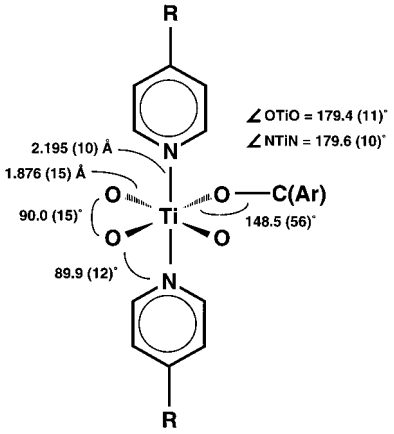

Figure 3. Average *trans*-$(ArO)_4TiL_2$ core.

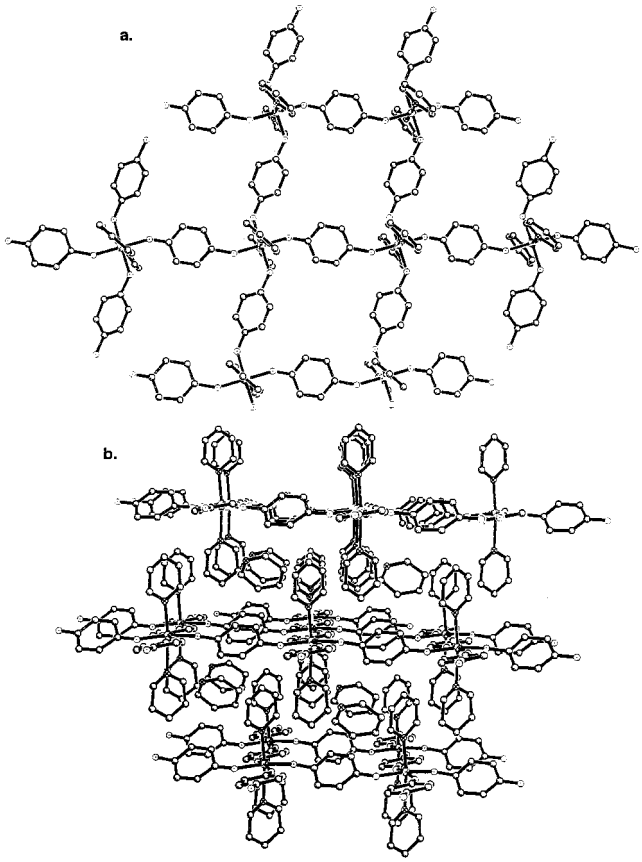

Figure 4. Flat sheet (a) of [*trans*-Ti($\mu_{1,4}$-$OC_6H_4O)_2py_2$·py]$_\infty$ (**3**-Ti), and its interpenetrating layers and intercalated pyridine (b).

expected that the ∠(TiOC) angles should show significant variation that reflects differing secondary structures, the 148.5-$(56)_{av}$° obtained for the four derivatives reveals only modest deviations from the norm.

4. [*trans*-Ti(μ-$OC_6H_4O)_2L_2]_\infty$ Secondary Structures. a. [*trans*-Ti($\mu_{1,4}$-$OC_6H_4O)_2py_2$·py]$_\infty$ (3-Ti). In Figure 4, the sheet structure of [*trans*-Ti($\mu_{1,4}$-$OC_6H_4O)_2$ py_2·py]$_\infty$ (**3**-Ti) is illustrated alone (a) and with neighboring sheets (b) that reveal void spaces partly filled by intercalated pyridine molecules. Both strands of *trans*-$\mu_{1,4}$-OC_6H_4O connections are slightly kinked at the oxygens (∠(TiOC) = $146.6(98)_{av}$°), and the phenyl rings are slightly canted with respect to the plane of titanium atoms, but these minor deviations do little to close the central void of the parallelogram. The void is filled by the interpenetration of pyridine residues from adjacent layers and the aforementioned pyridine.

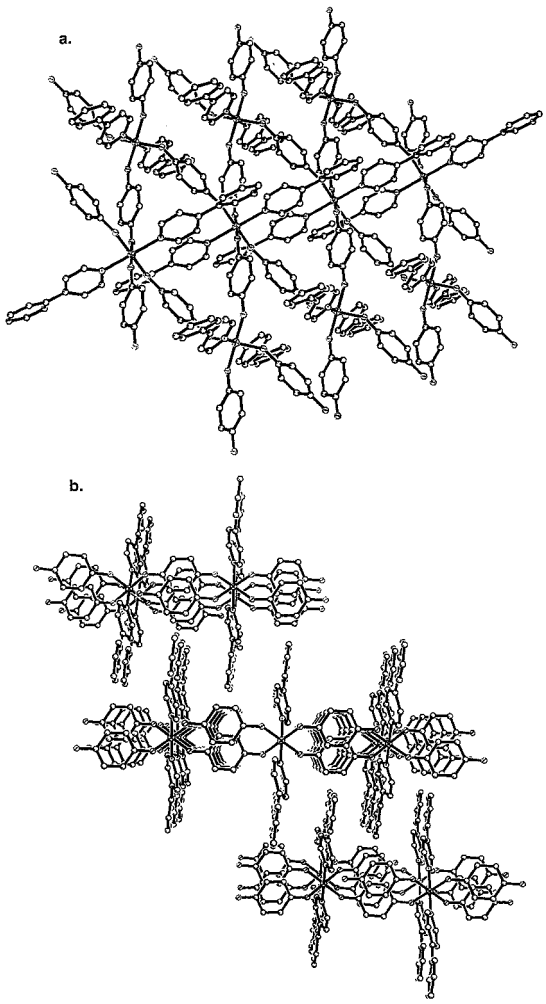

Figure 5. Rippled sheet of [*trans*-Ti($\mu_{1,4}$-$OC_6H_4O)_2$(4-Ph-py)$_2]_\infty$ (**4**-Ti) showing the alternating orientation of 4-Ph-py groups along the *trans*-1,4-OC_6H_4O connectivity (a), and the similarly disposed 4-phenylpyridines as viewed down each diagonal of the Ti_4($\mu_{1,4}$-$OC_6H_4O)_4$ parallelogram (b).

b. [*trans*-Ti($\mu_{1,4}$-$OC_6H_4O)_2$(4-Ph-py)$_2]_\infty$ (4-Ti). The depictions of the [*trans*-Ti($\mu_{1,4}$-$OC_6H_4O)_2$(4-Ph-py)$_2]_\infty$ (**4**-Ti) structure in Figure 5 show that use of the 4-phenylpyridine causes the flat sheets previously found for **3**-Ti to ripple in accommodating the added substituent. Within a strand of *trans*-$\mu_{1,4}$-OC_6H_4O-connected titanium centers, the O_4Ti planes tilt alternately such that the 4-phenylpyridines also alternate nearly 90° in their relative disposition (a). Consider the view down diagonally opposite, unconnected titanium centers of a Ti_4($\mu_{1,4}$-$OC_6H_4O)_4$ parallelogram (b). All of these titanium centers that comprise a single unconnected row possess the same tilt, and the orientations of 4-phenylpyridine are the same, while adjacent rows of titanium centers—similarly not directly connected by $\mu_{1,4}$-OC_6H_4O bridges—present the opposing tilt and requisite opposite orientation of 4-phenypyridine. This view also looks down the zigzag $\mu_{1,4}$-OC_6H_4O groups that connect dissimilar rows. The layers interpenetrate to minimize void space, and the phenyl residues on adjacent layers π-stack to pack efficiently.

c. [*trans*-Ti($\mu_{1,3}$-$OC_6H_4O)_2py_2]_\infty$ (5-Ti). A motif similar to that of **4**-Ti is exhibited by the resorcinol-derived [*trans*-Ti-($\mu_{1,3}$-$OC_6H_4O)_2py_2]_\infty$ (**5**-Ti). Figure 6 illustrates a related alternation of tilted titanium centers (a) and their correspondingly alternating pyridine ligands. The sheets are comprised of nearly rectangular Ti_4($\mu_{1,3}$-$OC_6H_4O)_4$ segments and are rippled due to the steric demands enforced by the 1,3-disposition of the

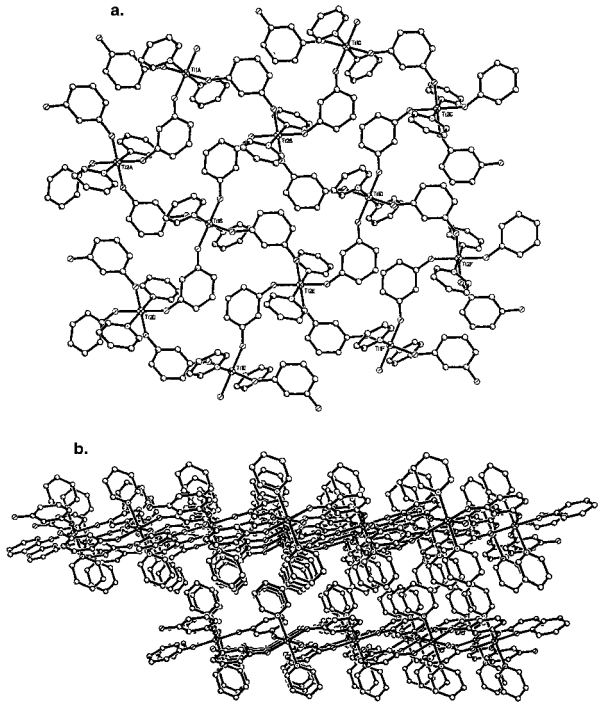

Figure 6. Rippled sheet of [*trans*-Ti($\mu_{1,3}$-$OC_6H_4O)_2py_2]_\infty$ (**5**-Ti) showing the alternating py orientations along the *trans*-1,3-OC_6H_4O connectivity (a), and the interpenetration of the sheets (b).

diaryloxide functionalities. A view across unconnected, diagonally opposed titanium centers reveals the like disposition of these units, but in these sheets adjacent rows have a related tilt in one direction (b), and alternating, opposing tilts in the orthogonal view. The interpenetration of adjacent layers is not as obvious for the relatively short pyridine residues in comparison to 4-phenylpyridine, but some π-stacking of the *ortho* and *meta* positions of the ligands is apparent.

d. [*trans*-Ti($\mu_{1,3}$-$OC_6H_4O)_2$(4-Ph-py)$_2]_\infty$ (6-Ti). [*trans*-Ti($\mu_{1,3}$-$OC_6H_4O)_2$(4-Ph-py)$_2]_\infty$ (**6**-Ti) features a combination of the more sterically restrictive $\mu_{1,3}$-OC_6H_4O bridge and the longer phenyl-substituted pyridine, and these different structural features appear to reinforce the patterns that emerged when they were observed separately. Figure 7 indicates essentially the same type of rippled sheet as in **5**-Ti (a), with the same alternation of O_4Ti planes. A greater interlayer interpenetration due to the longer 4-phenylpyridine residues is revealed (b), with the requisite π-stacking and as established in the structure of **4**-Ti.

Discussion

2-Dimensionality. In previous studies,[8−10] the combination of DHAs and molecular metal alkoxide precursors yielded CMONs based on dititanium edge-shared bioctahedral building blocks. In all but one highly restrictive case (i.e., the 2-dimensional {[Ti($\mu_{1,3}$-1,3-OC_6H_4O)(μ-1,3-OC_6H_4OH)(1,3-OC_6H_4OH)-(HO-^{i}Pr)]$_2$}$_n$),[10] 3-dimensional CMONs were produced, whose structural motifs were defined by the number of available linkers in the building block, and the nature of the bridging dialkoxyaromatic. With pyridine or a substituted pyridine present, these donors disrupt any potential aggregation of titanium centers, relegating the building block to a simple mononuclear *cis*- or *trans*-$(ArO)_4Tipy_2$ core. Clearly the μ-OAr and ArO$\cdots$HOAr bonds that hold the titanium centers in the edge-shared bioctahedral arrangement of the 3-dimensional CMON are significantly weaker than the common Ti−py bond. While it is difficult to be certain given the structural complexity evident, it is nonetheless likely that the change from dititanium to mononuclear building blocks in conjunction with the decrease in dimensionality is entropically favorable as well. Good donor solvents or ligands promote a decreased dimensionality in CMON systems based on early metals.

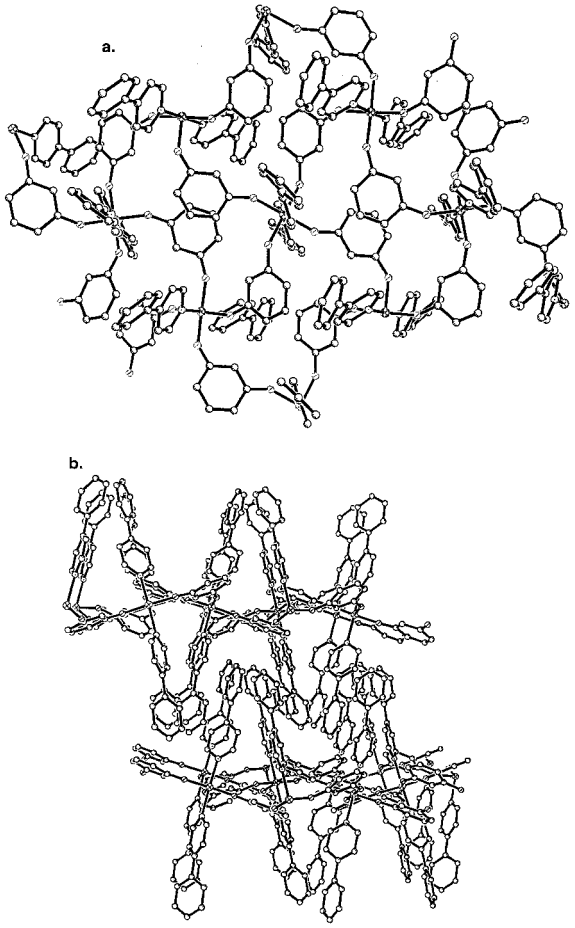

Figure 7. Rippled sheet of [*trans*-Ti($\mu_{1,3}$-$OC_6H_4O)_2$(4-Ph-py)$_2]_\infty$ (**6**-Ti) showing the alternating py orientations along the *trans*-1,3-OC_6H_4O connectivity (a), and the interpenetration of the sheets (b).

***cis*- versus *trans*-$(ArO)_4TiL_2$ Cores.** Contrary to expectations, mononuclear $(ArO)_4TiL_2$ complexes that would provide a logical structural comparison to the cores of the 2-dimensional CMONs are uncommon. Apparently such species are unstable relative to five-coordinate adducts, such as $(PhO)_4TiL$ (L = NH_3, NH_2Me, $NHMe_2$, NEt_3, py, etc.);[14] hence, the proclivity for *cis* versus *trans* coordination in six-coordinate complexes is uncertain. Given the strong *trans* influence typically accorded the aryloxide ligand, a *cis* geometry is probably expected unless counteracting steric interactions are significant. It follows that [*cis*-Ti($\mu_{1,4}$-$OC_6H_4O)_2py_2]_\infty$ (**2**-Ti) should be thermodynamically preferred over [*trans*-Ti($\mu_{1,4}$-$OC_6H_4O)_2py_2$·py]$_\infty$ (**3**-Ti), especially in consideration of the density issues previously described. It remains a mystery why the **3**-Ti is kinetically preferred in conditions of lower hydroquinone concentration. It is conceivable that trapping of solution-phase $(-OC_6H_4O)_4$Tipy oligomers by an additional py occurs more readily to give the *trans* core for steric reasons. Lower HOC_6H_4OH concentrations would then permit aggregation and crystallization to occur faster than isomerization.

While the observation of the *cis* geometry for [*cis*-Zr($\mu_{1,4}$-$OC_6H_4O)_2py_2]_\infty$ (**2**-Zr) could be ascribed to the same factors as

(14) Masthoff, R.; Köhler, H.; Böhland, H.; Schmeil, F. *Z. Chem.* **1965**, *5*, 122−130.

its titanium congener, the vanadium derivative possesses the [*trans*-V($\mu_{1,4}$-OC_6H_4O)$_2$py$_2$·py]$_\infty$ (**3**-V) structure, and all evidence indicates that this is the thermodynamic product. It is tempting to rationalize this set of observations on the size of the metal. Zirconium, whose bond lengths are ~0.1 Å greater than those of titanium, and ~0.2 Å longer than vandium's,[12] may more readily adopt the denser *cis* structure because of its greater size. The longer bond lengths may aid in the interlayer packing of the pleated sheets derived from the more restrictive *cis* core, while the void space in the alternative *trans* structure might be even greater in proportion to the size of zirconium, and far less energetically feasible. Both structure types are available to the intermediately sized titanium for the reasons espoused above, but the smaller vanadium may not be able to interlock the pleated sheets in the manner observed for **2**-Ti and presumed for **2**-Zr; its only alternative is the flat sheet structure, **3**-V. In accord with these arguments, the solid solutions, [*trans*-Ti$_x$V$_{1-x}$($\mu_{1,4}$-OC_6H_4O)$_2$py$_2$·py]$_\infty$ (**3**-Ti$_x$V$_{1-x}$, $x \approx 0.4, 0.6, 0.9$) conform to the *trans* structure due to the presence of vanadium. The varied bond lengths in the solid solutions should be easily accommodated through the flexibility of the M−O−C angles (i.e., 147° in **3**-Ti) in the *trans* geometry.

The remaining complexes all possess the *trans* core, but the added restrictions of the 1,3-OC_6H_4O− bridges and substituted py adducts appear to eliminate the *cis* structure from consideration. The "rippling" intrinsic to the sheets derived from resorcinol essentially makes the 2-dimensional net denser. It is likely that a similar occurrence in the *cis* configuration would render impossible the type of interpenetration observed for **2**-Ti. In the *trans* geometry, interpenetration by the more constricted rippled sheets obviates the need for an intercalated py, as found in **3**-M (M = Ti, V). The 4-phenylpyridine ligands appear to rule out the pleated sheet *cis* geometry, because interpenetration of these bulky residues cannot be accommodated within this structure type.

It remains to be seen whether the purported stability of the *cis*- rather than *trans*-(ArO)$_4$TiL$_2$ core can play a greater role in determining the ultimate structure type of a CMON system. For the derivatives herein, the core geometry appears to be secondary in importance relative to steric, packing, or interpenetration constraints that ultimately control the density of the solid. As a corollary, the inability to intercalate simple aromatic hydrogens, etc. into the 2-dimensional CMON, with the minor exception of the benzene/pyridine exchange observed for **3**-Ti, must be a direct consequence of the ready interpenetration of the various layers.[13] As previously noted, **3**-Ti is the least dense of the titanium-derived 2-dimensional CMONs, and already possesses an intercalated pyridine that undergoes exchange.

Summary

The use of pyridine and substituted pyridines (L) in CMON syntheses with 1,4- and 1,3-dihydroxybenzene and various metal alkoxides obviates the formation of the diniuclear, bioctahedral building block common to previously studied 3-dimensional titanium derivatives. The resulting mononuclear (ArO)$_4$ML$_2$ cores afford 2-dimensional materials that assume layered structures. Interpenetration of the pleated sheets of the *cis* core (**2**-Ti) and a similar packing of rippled and planar sheets derived from *trans* cores provide the main impetus toward dense networks that are effectively devoid of intercalation chemistry.

Experimental Section

General Considerations. All manipulations were performed on a high-vacuum line or in an inert atmosphere drybox unless otherwise noted. Tetrahydrofuran was distilled from purple sodium benzophenone ketyl and then vacuum transferred from the same into a glass bomb immediately prior to use in the drybox. Pyridine was refluxed over sodium, subsequently vacuum transferred onto activated 4 Å molecular sieves, and vacuum transferred into a glass bomb for storage in the drybox. Hydroquinone (Aldrich, 99+%) and resorcinol (Aldrich, 99+%) were dried by dissolving in dry THF and removing the volatiles; this procedure was repeated three times. 4-Phenylpyridine (Aldrich, 97%), Ti(O^{i}Pr)$_4$ (Aldrich, 97%), and Zr(OEt)$_4$ (Strem Chemicals, 99+%) were used as received and stored in the drybox. V(O^{i}Pr)$_4$ was prepared by the literature method[15] as was Ti(N(TMS$_2$))$_3$.[16] Titanium−hyroquinone precursor **1**-Ti was prepared as previously described.[8] DCl (20 wt % in D_2O, Aldrich), D_2O (Cambridge Isotope Laboratories, 99.9% D), and CD_3OD (Cambridge Isotope Laboratories, 99.8% D) were used as received; solutions for ^{1}H NMR spectra were ca. 3 wt % DCl (~1 M) and were prepared on the benchtop.

^{1}H NMR spectra were obtained on a Varian XL-200 spectrometer. Spectra were the product of four transients with a 60 s delay between acquisitions to ensure accurate integrations. Powder diffraction was performed on a Scintag XRD system interfaced to a Digital MicroVax computer or PC with Windows NT. Standard powder patterns were recorded as continuous scans with a chopper increment of $2\theta = 0.03°$ and a scan rate of 2 deg/min. When crystal quality permitted, patterns for indexing and refinement of unit cell parameters were recorded at 0.03° steps in 2θ, with diffraction recorded for at least 30 s at each step. Patterns were indexed using TREOR or VISSER, and unit cell constants were refined using LATCON, all part of the Proszki suite of programs. Electron probe microanalysis was performed on a JEOL 733 electron microscope operating at an accelerating voltage of 15 kV.

Procedures. 1. Preparation of [V(OC_6H_4O)$_a$(OC_6H_4OH)$_{3.33-1.83a}$-(O^{i}Pr)$_{0.66-0.17a}$(THF)$_{\sim 0.2}$]$_n$ (1-V). Hydroquinone (1.15 g, 10.4 mmol) was placed in a 100 mL round-bottom flask on a swivel frit, and V(O^{i}Pr)$_4$ (1.00 g, 3.48 mmol) was placed in another 100 mL flask. THF (~30 mL) was vacuum transferred into each flask to form a colorless and a dark blue solution, respectively. The V(O^{i}Pr)$_4$ solution was taken up by syringe and added to the hydroquinone under argon counterflow. A black precipitate resulted, and the mixture was stirred for 3 h at 22 °C. The suspension was filtered, and the volatiles were removed. The black paste was triturated with hexanes to obtain a black powder on the removal of all volatiles under active vacuum. ^{1}H NMR spectra of samples degraded in D_2O/DCl suggested a rough empirical formula similar to that of **1**-Ti: V(OC_6H_4O)$_a$(OC_6H_4-OH)$_{3.33-1.83a}$(O^{i}Pr)$_{0.66-0.17a}$(THF)$_{\sim 0.2}$ ($0.90 \le a \le 1.82$).

2. Preparation of [Zr(OC_6H_4O)$_{2-x}$(OEt)$_{2x}$]$_n$ (1-Zr). Hydroquinone (1.00 g, 9.1 mmol) was placed in a 250 mL round-bottom flask and dissolved in THF (~30 mL). Zr(OEt)$_4$ (1.00 g, 3.7 mmol) was placed in another 100 mL flask into which THF (~60 mL) was vacuum transferred to form a fine suspension. The Zr(OEt)$_4$ suspension was taken up by syringe and added to the hydroquinone under argon counterflow. The mixture was stirred overnight at 22 °C, resulting in a white precipitate. More precipitate was obtained by reducing the volume of solvent, and the suspension was filtered, the volatiles were removed, and the product was dried under active vacuum for 5 h. A ^{1}H NMR spectrum of a sample degraded in D_2O/DCl yielded the empirical formula Zr(OC_6H_4O)$_{2-x}$(OEt)$_{2x}$, where $x \approx 0.9$.

3. Preparation of [*cis*-Ti($\mu_{1,4}$-OC_6H_4O)$_2$py$_2$]$_\infty$ (2-Ti). Hydroquinone (1.50 g, 13.6 mmol), 250 mg of **1**-Ti, and 7.5 mL of pyridine (1.8 M hydroquinone) were combined in a glass bomb and heated to 100 °C for 96 h. The resulting red microcrystals were collected on a glass frit on the benchtop, washed with pyridine, and placed under vacuum for 15 min. A ^{1}H NMR spectrum of the material quenched by D_2O/DCl revealed a 1:1 ratio of hydroquinone to pyridine. The powder XRD matched the theoretical pattern generated from the single-crystal diffraction data, with no extraneous peaks. Anal. Calcd for $C_{22}H_{18}O_4N_2$-Ti (Found): C, 62.57 (62.12); H, 4.30 (4.05); N, 6.63 (6.41). IR (Nujol, cm^{-1}): 1603 (m), 1203 (vs, br), 1152 (m), 1084 (m), 1068 (m), 1040 (m), 1011 (m), 887 (m), 832 (vs), 828 (vs), 757 (m), 711 (m), 698 (m), 629 (m), 528 (m), 521 (m), 479 (m), 444 (vs), 429 (s).

(15) Bradley, D. C.; Mehta, M. L. *Can. J. Chem.* **1962**, *40*, 1183−1188.
(16) Bradley, D. C.; Copperthwaite, R. G. *Inorg. Synth.* **1978**, *18*, 112−120.
(17) Schmidt, G. M. J. *Pure Appl. Chem.* **1971**, *27*, 647−679.

4. Preparation of [*cis*-Zr($\mu_{1,4}$-$OC_6H_4O)_2py_2]_\infty$ (2-Zr). Hydroquinone (3.0 g, 27.3 mmol), 300 mg of **1**-Zr, and 25 mL of pyridine (1.1 M hydroquinone) were combined in a glass bomb and heated to 100 °C for 7 d. The resulting white powder was collected on a glass frit, washed with THF, and placed under vacuum for ~30 min. A ^{1}H NMR spectrum (D_2O/DCl) of the degraded compound confirmed the 1:1 ratio of hydroquinone to pyridine and the absence of EtOD. Its powder pattern correlated with that of $[Ti(1,4\text{-}OC_6H_4O)_2(py)_2]_\infty$ (**2**-Ti), and was indexed to an orthorhombic cell with a = 15.731(6) Å, b = 14.290(7) Å, c = 9.292(4) Å, and V = 2088.9 Å^3.

5. Preparation of [*trans*-Ti($\mu_{1,4}$-$OC_6H_4O)_2py_2$·py]$_\infty$ (3-Ti). Hydroquinone (1.5 g, 13.6 mmol), 250 mg of **1**-Ti, and 25 mL of pyridine (0.55 M hydroquinone) were combined in a glass bomb and heated to 100 °C for 7 d. A black solid with a green tint was isolated on a glass frit on the benchtop, washed with pyridine, and placed under vacuum for 15 min. A ^{1}H NMR spectrum of a sample degraded in D_2O/DCl indicated a 2:3 ratio of DOC_6H_4OD to py. Inspection of a few milligrams of crystals in Paratone oil under a microscope revealed light blue-green crystals <5 μm on a side. Powder diffraction revealed no **2**-Ti, and the data were indexed to a triclinic unit cell: a = 8.717(2) Å, b = 8.803(2) Å, c = 9.016(2) Å, α = 82.83(2)°, β = 75.36(2)°, γ = 71.09(2)°, V = 632.6 Å^3. Anal. Calcd for $C_{27}H_{23}O_4N_3Ti$ (Found): C, 64.68 (63.27); H, 4.62 (4.44); N, 8.38 (7.70). IR (Nujol, cm^{-1}): 1604 (m), 1225 (vs), 1152 (m), 1090 (w), 1069 (m), 1041 (m), 1014 (m), 839 (vs), 759 (w), 744 (w), 723 (w), 701 (m), 694 (m), 651 (w), 638 (m), 526 (w), 450 (s), 421 (m). Larger crystals of **3**-Ti that proved suitable for a single-crystal X-ray structure determination were obtained in the following manner. Hydroquinone (172 mg, 1.56 mmol) was placed in a 50 mL round-bottom flask, and $Ti(N(SiMe_3)_2)_3$ (500 mg, 0.95 mmol) was placed in another 50 mL flask. THF (~20 mL) was vacuum transferred onto the $Ti(N(SiMe_3)_2)_3$ and onto the hydroquinone (~12 mL). The blue $Ti(N(SiMe_3)_2)_3$ solution was taken up by syringe and added to the hydroquinone under argon counterflow. A brown-orange solution and precipitate immediately resulted, and the mixture was stirred for 7 h at 22 °C. The precipitate was filtered from a light yellow solution and triturated three times with THF, and the volatiles were removed. A ^{1}H NMR spectrum of a sample degraded in D_2O/DCl yielded the empirical formula $Ti(OC_6H_4O)_{1.5-x}(N(SiMe_3)_2)_{2x}(THF)_{\sim 0.6}$ with $2x \approx 0.03$. This solid (47 mg), hydroquinone (400 mg, 3.6 mmol), and 2 mL of pyridine were combined in a glass tube, sealed under vacuum, and heated at 85 °C for 3 d. The bulk dark green product with shiny gold metallic crystals was collected by filtration, washed with THF, and dried under active vacuum for 10 min. The powder pattern matched that of the material prepared from the Ti(IV) precursor, and a ^{1}H NMR spectrum of a sample degraded in D_2O/DCl confirmed the 2:3 ratio of DOC_6H_4OD to py.

6. Preparation of [*trans*-V($\mu_{1,4}$-$OC_6H_4O)_2py_2$·py]$_\infty$ (3-V). Hydroquinone (3.0 g, 27.3 mmol), 300 mg of **1**-V, and ~8 mL of py (3.4 M hydroquinone) were combined in a glass bomb and heated to 100 °C for 13 d. The product was filtered on a glass frit, washed with THF, and dried under active vacuum for 20 min. A ^{1}H NMR spectrum confirmed the 2:3 ratio of hydroquinone to pyridine, and the powder XRD correlated with that of **3**-Ti. The powder pattern was indexed to a triclinic unit cell: a = 8.355(2) Å, b = 8.765(2) Å, c = 8.925(2) Å, α = 84.14(5)°, β = 79.19(5)°, γ = 76.25(2)°, V = 622.5 Å^3. Magnetic susceptibility experiments showed the compound to be paramagnetic from 298 to 2 K, μ = 2.06(6) μ_B.

7. Preparation of $[Ti_xV_{1-x}(1,4\text{-}OC_6H_4O)_2(py)_2$·(py)]$_\infty$ (3-Ti_xV_{1-x}, $x \approx$ 0.4, 0.6, 0.9). Hydroquinone (3 g, 0.027 mmol) was placed in a glass bomb with the respective portions of **1**-Ti (75 mg, 150 mg, or 225 mg) and **1**-V (225 mg, 150 mg, or 75 mg) given. The bomb was degassed, pyridine (~15 mL) was added via vacuum transfer, and the bomb was heated for 2 d at 100 °C. The dark, olive drab powder obtained in each case was collected on a frit, washed twice with THF (~15 mL), and dried by vacuum (~20 m). Inspection of the material in Paratone oil by light microscopy revealed it to be ~50% microcrystalline, with the larger crystals appearing red-orange and the smaller crystals blue-green; none were larger than 20 μm. ^{1}H NMR samples of **3**-Ti_xV_{1-x} degraded in D_2O/DCl afforded a 2:3 ratio of DOC_6H_4OD to py. Powder XRD patterns matched those of **3**-Ti and **3**-V with peaks slightly shifted in 2θ. The pattern of **3**-$Ti_{0.6}V_{0.4}$ was indexed to a triclinic unit cell with a = 8.600(5) Å, b = 8.782(4) Å, c = 8.965(6) Å, a = 83.13(5)°, b = 76.26(6)°, c = 72.61(6)°, and V = 626.8 Å^3. Electron probe microanalysis of **3**-$Ti_{0.6}V_{0.4}$, operating in spot mode on 42 different single crystals (both colors), gave the average atom % Ti and atom % V as 60(7) and 40(7), respectively. An average of two analyses of bulk samples of **3**-$Ti_{0.6}V_{0.4}$ gave the atom % Ti as 57(2) and the atom % V as 43(2). One analysis of a bulk sample of **3**-$Ti_{0.4}V_{0.6}$ provided the % Ti:% V as 38:62, and one analysis of a bulk sample of **3**-$Ti_{0.9}V_{0.1}$ provided the % Ti:% V as 90:10.

8. Preparation of [*trans*-Ti($\mu_{1,4}$-$OC_6H_4O)_2$(4-Ph-py)$_2]_\infty$ (4-Ti). Ti($O^iPr)_4$ (300 mg, 1.1 mmol), hydroquinone (300 mg, 2.7 mmol) and 4-phenylpyridine (2.0 g, 12.9 mmol) were placed in a 10 mm o.d. glass tube which was then sealed under vacuum. The tube was heated at 100 °C for 2 months, although crystals were observed after several days. The bulk forest green product with lustrous metallic crystals was collected by filtration, washed with THF, and dried under active vacuum for a few minutes. A ^{1}H NMR spectrum of a sample degraded in CD_3OD/DCl indicated a 2:3 ratio of DOC_6H_4OD to 4-Ph-py, which is inconsistent with the crystal structure obtained from single-crystal X-ray diffraction. Inspection of a sample in Paratone oil under a microscope revealed the product to be ~20% red-orange rectangular block crystals mixed with a dark opaque powder. The X-ray powder pattern of the bulk matched the theoretical pattern of **4**-Ti obtained from the single-crystal X-ray diffraction data; hence, the dark powder was assumed to be amorphous.

9. Preparation of [*trans*-V($\mu_{1,4}$-$OC_6H_4O)_2$(4-Ph-py)$_2]_\infty$ (4-V). V($O^iPr)_4$ (200 mg, 0.70 mmol), hydroquinone (307 mg, 2.8 mmol), and 4-phenylpyridine (~2.0 g, 12.9 mmol) were placed in a glass tube which was then sealed under vacuum. The tube was heated at 100° C for 6 months, although crystals were observed after several days. The bulk forest green product was collected by filtration, washed with THF, and dried under vacuum. A ^{1}H NMR spectrum of a sample dissolved in CD_3OD/DCl indicated a 2:2.25 ratio of DOC_6H_4OD to 4-Ph-py, inconsistent with the crystal structure of the Ti analogue **4**-Ti. Inspection of a sample in Paratone oil under a microscope revealed the product to be ~50% yellow crystals mixed with a dark opaque powder. The X-ray powder pattern of the bulk correlated with the theoretical pattern of the Ti analogue **4**-Ti with no extraneous peaks.

10. Preparation of [*trans*-Ti($\mu_{1,3}$-$OC_6H_4O)_2py_2]_\infty$ (5-Ti). Ti($O^iPr)_4$ (100 mg, 0.35 mmol) was added to a suspension of resorcinol (500 mg, 4.5 mmol) and pyridine (~3 mL) in a glass tube to give a yellow-orange solution. The tube was sealed under vacuum and heated at 100° C for 2 d, resulting in large red crystals that were collected by filtration, washed with THF on the benchtop, and immediately dried in vacuo for ~10 min. Inspection of a sample in Paratone oil under a microscope revealed the crystals to be red-orange flakes of various shapes. Powder XRD matched the theoretical pattern obtained from single-crystal diffraction studies of **5**-Ti. A ^{1}H NMR spectrum of a sample degraded in D_2O/DCl indicated a 1:1 ratio of DOC_6H_4OD to py. Anal. Calcd for $C_{22}H_{18}O_4N_2Ti$ (Found): C, 62.57 (62.82); H, 4.30 (4.28); N, 6.63 (6.56). IR (Nujol, cm^{-1}): 1603 (m), 1575 (s), 1563 (s), 1557 (s), 1300 (s), 1288 (s), 1248 (s), 1215 (m), 1170 (vs), 1153 (s), 1132 (vs), 1067 (m), 1041 (m), 1010 (m), 974 (vs, br), 884 (w), 872 (m), 863 (m), 821 (s), 787 (w), 766 (m), 762 (m), 756 (m), 724 (w), 695 (s), 655 (s), 638 (vs, br), 502 (m), 437 (s), 404 (s).

11. Preparation of [*trans*-Ti($\mu_{1,3}$-$OC_6H_4O)_2$(4-Ph-py)$_2]_\infty$ (6-Ti). Ti($O^iPr)_4$ (1.0 g, 3.5 mmol), resorcinol (1.0 g, 9.1 mmol), and 4-phenylpyridine (6.25 g, 40 mmol) were placed in a glass bomb and heated at 100 °C for 4 weeks. Large, deep red crystals were collected by filtration, washed with THF, and dried under vacuum for 30 min. A ^{1}H NMR spectrum of a sample degraded in CD_3OD/DCl indicated a 1:1 ratio of DOC_6H_4OD to 4-Ph-py, and the X-ray powder pattern of the bulk matched the theoretical pattern obtained from single-crystal X-ray diffraction data of **6**-Ti. Anal. Calcd for $C_{34}H_{26}O_4N_2Ti$ (Found): C, 71.15 (70.88); H, 4.53 (5.04); N, 4.88 (5.04). IR (Nujol, cm^{-1}): 1613 (m), 1574 (s), 1563 (s), 1557 (s), 1300 (s), 1290 (s), 1249 (s), 1224 (w), 1197 (w), 1167 (s), 1133 (s), 1074 (w), 1068 (w), 1045 (w), 1030 (w), 1013 (w), 994 (w), 975 (s, br), 875 (m), 853 (m), 843 (s), 819 (s), 765 (m), 759 (m), 731 (m), 690 (m), 681 (w), 666 (m), 635 (s, br), 624 (s, br), 557 (m), 509 (m), 502 (m), 497 (m), 480 (m), 417 (m).

Single-Crystal X-ray Structure Determinations. 12. [*cis*-Ti($\mu_{1,4}$-$OC_6H_4O)_2py_2]_\infty$ (2-Ti). Crystals were grown from pyridine as explained above. A few milligrams of crystals were suspended in Paratone oil on a glass slide. Handling the crystals in Paratone for a few hours in the ambient atmosphere caused no apparent decomposition. Under a microscope, a single diamond-shaped crystal was isolated in a rayon fiber loop epoxied to a glass fiber.[18,19] On the A1 line at the Cornell High Energy Synchrotron Source (CHESS), the crystal was frozen in a 110 K nitrogen stream. The crystal-to-detector distance was set at 43 mm. A 2K CCD was used to record diffraction.[20] Data were collected as 20 s, 15° oscillations in ϕ, with a total of 360° collected. Observed intensities were corrected for Lorentz and polarization effects; no absorption correction was applied. The first frame was indexed using the program DENZO,[21] and all the data were scaled together with SCALEPACK. The structure was solved by direct methods (SHELXS), and hydrogen atoms were added geometrically. The structure was refined by full-matrix least-squares on F^2 (SHELX-93) using anisotropic thermal parameters for all non-hydrogen atoms.

13. [*trans*-Ti($\mu_{1,4}$-$OC_6H_4O)_2py_2$·py]$_\infty$ (3-Ti). Crystals large enough for structure determination were grown from pyridine as explained above. A few milligrams of crystals was suspended in Paratone oil on a glass slide. Under a microscope, a single red-orange, elongated hexagon-shaped plate was epoxied to a 1 mm length of glass wool which was previously attached to a thin glass fiber. X-ray diffraction data were collected on a Siemens SMART system employing a 1K CCD detector and an Oxford Cryostream set at 146 K. Observed intensities were corrected for Lorentz and polarization effects, and a semiempirical absorption correction was applied (SADABS). The structure was solved by direct methods (SHELXTL) in $P1$, and after some initial refinement transferred to $P\bar{1}$. Hydrogen atoms were added geometrically. The structure was refined by full-matrix least-squares on F^2 using anisotropic thermal parameters for all non-hydrogen atoms.

14. [*trans*-Ti($\mu_{1,4}$-$OC_6H_4O)_2$(4-Ph-py)$_2]_\infty$ (4-Ti). Crystals were grown from 4-phenylpyridine as explained above, and one was mounted with epoxy on a glass fiber. X-ray diffraction data were collected on a Siemens SMART system employing a 1K CCD detector at 23 °C. Observed intensities were corrected for Lorentz and polarization effects, and a semiempirical absorption correction was applied (SADABS). The structure was solved by direct methods (SHELXTL), and all hydrogen atoms were located in the difference Fourier map. The structure was refined by full-matrix least-squares on F^2 using anisotropic thermal parameters for all non-hydrogen atoms.

15. [*trans*-Ti($\mu_{1,3}$-$OC_6H_4O)_2py_2]_\infty$ (5-Ti). Crystals were grown from pyridine as explained above. A roughly rectangular orange flake was mounted with epoxy on a glass fiber and subsequently dipped in epoxy to coat. X-ray diffraction data were collected on a Siemens SMART system employing a 1K CCD detector at 23 °C. Observed intensities were corrected for Lorentz and polarization effects, and a semiempirical absorption correction was applied (SADABS). The structure was solved by direct methods (SHELXTL). Hydrogen atoms were added geometrically. The structure was refined by full-matrix least-squares on F^2 using anisotropic thermal parameters for all non-hydrogen atoms.

16. [*trans*-Ti($\mu_{1,3}$-$OC_6H_4O)_2$(4-Ph-py)$_2]_\infty$ (6-Ti). Crystals were grown from 4-phenylpyridine as explained above. A large trigonal prism was stuck to a copper needle with Paratone oil. X-ray diffraction data were collected on a Siemens SMART system employing a 1K CCD detector and an Oxford Cryostream operating at 173 K. Observed intensities were corrected for Lorentz and polarization effects, and a semiempirical absorption correction was applied (SADABS). The structure was solved by direct methods (SHELXTL), and all hydrogen atoms were located in the difference Fourier map. The structure was refined by full-matrix least-squares on F^2 using anisotropic thermal parameters for all non-hydrogen atoms.

Acknowledgment. We thank John M. Pette for experimental assistance. We gratefully acknowledge contributions from the National Science Foundation (Grant CHE-9816134, Inorganic Materials Traineeship to T.P.V. (Grant DMR-9256824), Cornell High Energy Synchrotron Source (CHESS), Cornell Center for Materials Research (DMR-9632275), MSC REU to J.P.), and Cornell University.

Supporting Information Available: X-ray structural data pertaining to [*trans*-Ti($\mu_{1,4}$-$OC_6H_4O)_2py_2$·py]$_\infty$ (**3**-Ti), [*trans*-Ti($\mu_{1,4}$-$OC_6H_4O)_2$(4-Ph-py)$_2]_\infty$ (**4**-Ti), [*trans*-Ti($\mu_{1,3}$-$OC_6H_4O)_2py_2]_\infty$ (**5**-Ti), and [*trans*-Ti($\mu_{1,3}$-$OC_6H_4O)_2$(4-Ph-py)$_2]_\infty$ (**6**-Ti): a summary of crystallographic parameters, atomic coordinates, bond distances and angles, and anisotropic thermal parameters. This material is available free of charge via the Internet at http://pubs.acs.org. The X-ray structural information pertaining to [*cis*-Ti($\mu_{1,4}$-$OC_6H_4O)_2py_2]_\infty$ (**2**-Ti) (**2**) may be found as Supporting Information to ref 9.

IC0003473

(18) Blond, L.; Pares, S.; Kahn, R. *J. Appl. Crystallogr.* **1995**, *28*, 653−654.

(19) A thorough explanation of the construction of fiber loops and experimental methods at CHESS is given in Walter, R. L. Ph.D. Thesis, Cornell University, 1996.

(20) (a) Thiel, D. J.; Walter, R. L.; Ealick, S. E.; Bilderback, D. H.; Tate, M. W.; Gruner, S. M.; Eikenberry, E. F. *Rev. Sci. Instrum.* **1995**, *3*, 835−844. (b) Walter, R. L.; Thiel, D. J.; Barna, S. L.; Tate, M. W.; Wall, M. E.; Eikenberry, E. F.; Gruner, S. M.; Ealick, S. E. *Structure* **1995**, *3*, 835−844.

(21) Otwinski, Z. DENZO, a program for automatic evaluation of film densities, Department for Molecular Biophysics and Biochemistry, Yale University, New Haven, CT, 1988.